

Comparative study of field-dependent carrier dynamics and emission kinetics of InGaN/GaN light-emitting diodes grown on (11 2⁻²) semipolar versus (0001) polar planes

Yun Ji, Wei Liu, Talha Erdem, Rui Chen, Swee Tiam Tan, Zi-Hui Zhang, Zhengang Ju, Xueliang Zhang, Handong Sun, Xiao Wei Sun, Yuji Zhao, Steven P. DenBaars, Shuji Nakamura, and Hilmi Volkan Demir

Citation: *Applied Physics Letters* **104**, 143506 (2014); doi: 10.1063/1.4870840

View online: <http://dx.doi.org/10.1063/1.4870840>

View Table of Contents: <http://scitation.aip.org/content/aip/journal/apl/104/14?ver=pdfcov>

Published by the *AIP Publishing*

Articles you may be interested in

Ultraviolet light-emitting diodes grown by plasma-assisted molecular beam epitaxy on semipolar GaN (20 2⁻¹) substrates

Appl. Phys. Lett. **102**, 111107 (2013); 10.1063/1.4796123

High optical polarization ratio from semipolar (20 2⁻¹) blue-green InGaN/GaN light-emitting diodes

Appl. Phys. Lett. **99**, 051109 (2011); 10.1063/1.3619826

High power and high efficiency blue light emitting diode on freestanding semipolar (10 1⁻¹) bulk GaN substrate

Appl. Phys. Lett. **90**, 233504 (2007); 10.1063/1.2746418

Light-polarization characteristics of electroluminescence from InGaN/GaN light-emitting diodes prepared on (11 2⁻²) -plane GaN

J. Appl. Phys. **100**, 113109 (2006); 10.1063/1.2382667

Demonstration of a semipolar (10 1⁻³) InGaN/GaN green light emitting diode

Appl. Phys. Lett. **87**, 231110 (2005); 10.1063/1.2139841



physicstoday

Comment on any
Physics Today article.

Physics Today / Volume 63 / Issue 1 / July 2012
Previous Article | Next Article
Measured energy in Japan
David von Seggern
(vonseg@esemr.unr.edu) University of Nevada
July 2012, page 10
DIGITAL OBJECT IDENTIFIER
<http://dx.doi.org/10.1063/PFT.3.1619>
The article by Thome Lay and Hiroo Kanamori is an excellent review of the energy released by the 2011 Tohoku earthquake. While that of a 100-megaton nuclear explosion is approximately five times as much energy as that of a 100-megaton atmospheric explosion, the 1964 Chilean earthquake had still more energy by a factor of about 3, or 15 times that of a nuclear device. I believe the authors used the relation for seismic energy release rather than total strain energy release. The seismic energy underestimates the total strain energy release by a variable that depends on friction on the fault plane. Accounting for total strain energy release would increase the earthquake energy number by orders of magnitude.
Despite the catastrophic damage potential of nuclear bombs, the forces of nature occasionally unleash much larger energy releases. Although the nuclear bombs are under our control, earthquakes, volcanic eruptions, and extreme weather events are not. However, by judicious preparation and avoidance measures, humans can significantly diminish the damage of natural events.
This article does not have any references.
Comment on this article
By the act of hitting a ball with a bat, one calculates the force energy to deliver the ball to its new location, but one must also take into account that the bat extended its energy release to that which became struck by the ball as its momentum ceased and passed energy to the struck item. Therefore the parameters of the damage extend into the future when the received energy to that pushed upon, later becomes released in a new event. Perhaps calculations of one added that in while another's calculations did not. E.M.C.
Written by Edgar McCarville, 14 July 2012 19:59

Comparative study of field-dependent carrier dynamics and emission kinetics of InGaN/GaN light-emitting diodes grown on (11 $\bar{2}$ 2) semipolar versus (0001) polar planes

Yun Ji,¹ Wei Liu,¹ Talha Erdem,² Rui Chen,¹ Swee Tiam Tan,¹ Zi-Hui Zhang,¹ Zhengang Ju,¹ Xueliang Zhang,¹ Handong Sun,¹ Xiao Wei Sun,¹ Yuji Zhao,³ Steven P. DenBaars,^{3,a)} Shuji Nakamura,³ and Hilmi Volkan Demir^{1,2,a)}

¹LUMINOUS! Centre of Excellence for Semiconductor Lighting and Displays, School of Electrical and Electronic Engineering, School of Physical and Mathematical Sciences, Nanyang Technological University, 50 Nanyang Avenue, Singapore 639798

²Department of Electrical and Electronics, Department of Physics, and UNAM–Institute of Material Science and Nanotechnology, Bilkent University, Ankara TR-06800, Turkey

³Electrical and Computer Engineering and Materials Department, University of California, Santa Barbara, California 93106, USA

(Received 26 February 2014; accepted 28 March 2014; published online 9 April 2014)

The characteristics of electroluminescence (EL) and photoluminescence (PL) emission from GaN light-emitting diodes (LEDs) grown on (11 $\bar{2}$ 2) semipolar plane and (0001) polar plane have been comparatively investigated. Through different bias-dependent shifting trends observed from the PL and time-resolved PL spectra (TRPL) for the two types of LEDs, the carrier dynamics within the multiple quantum wells (MQWs) region is systematically analyzed and the distinct field-dependent emission kinetics are revealed. Moreover, the polarization induced internal electric field has been deduced for each of the LEDs. The relatively stable emission behavior observed in the semipolar LED is attributed to the smaller polarization induced internal electric field. The study provides meaningful insight for the design of quantum well (QW) structures with high radiative recombination rates. © 2014 AIP Publishing LLC. [<http://dx.doi.org/10.1063/1.4870840>]

III-Nitride light-emitting diodes (LEDs) have shown enormous potential as high efficiency light sources for full-color display and solid-state lighting. The traditional growth of InGaN/GaN multiple quantum well (MQW) LEDs mainly focuses on structures grown along the *c*-axis orientation, which is perpendicular to the growth plane.^{1–3} The MQWs grown along this orientation suffer from spontaneous and piezoelectric polarizations, which induce an internal electric field and tilt the energy bands of the QWs, and spatially separate the electron and hole wave functions, leading to reduced oscillator strength due to the quantum-confined Stark effect (QCSE). Consequently, the radiative recombination rate within the MQWs is suppressed, limiting the efficiency of LED devices. Moreover, as a result, the emission peak wavelength shifts under different bias currents. To eliminate the undesirable influences by the polarization fields, growing LED structures on nonpolar or semipolar planes has been proposed to minimize the QCSE.^{4–8} The device structures grown on the semipolar and nonpolar planes present a more stable performance, and are supposed to enable a higher efficiency compared to the devices based on [0001] orientation. However, to date, the mechanism of how the polarization field influences the carrier recombination and hence affects the performance of the devices in the semipolar *versus* polar structures is unknown.

In this work, the electroluminescence (EL) and photoluminescence (PL) emission performances of LED devices grown on (11 $\bar{2}$ 2) semipolar and (0001) polar planes are

comparatively studied with the assistance of electroabsorption measurements. The semipolar LED devices are found to exhibit more stable EL and PL emissions, as compared to the polar LED devices. Furthermore, when the devices are biased with external voltage, the PL emission peaks of the polar and semipolar devices are, surprisingly, observed to present opposite shifting trends. Time-resolved PL (TRPL) measurement reveals that the semipolar LED device has a much shorter carrier lifetime compared to the polar LED device. The strength of polarization induced internal electric field is indirectly estimated through the external bias condition. The performance difference for the polar and semipolar LED devices is attributed to the different polarization induced internal electric fields originating from the polar and semipolar growth planes.

Two blue InGaN/GaN LED wafers were grown using the metal-organic chemical vapor deposition (MOCVD) system. The polar GaN LED sample was grown on the (0001) *c*-plane sapphire substrate, while the semipolar LED sample was grown on the (11 $\bar{2}$ 2) *r*-plane GaN substrate. Both epitaxial structures consist of a 30 nm thick low temperature buffer layer, a 4 μ m thick unintentionally doped bulk GaN layer, a 2 μ m thick Si-doped n-GaN layer, five pairs of InGaN/GaN QWs, with quantum well and barrier thickness of 3 nm and 12 nm, respectively, and finally a 200 nm thick Mg-doped p-GaN layer. The doping concentrations of the n-GaN and p-GaN layers were $5 \times 10^{18}/\text{cm}^3$ and $3 \times 10^{17}/\text{cm}^3$, respectively.

After growth, the epi-wafers were further fabricated into chips using standard device fabrication process. A Ni/Au layer with 5 nm/5 nm thickness was deposited and annealed

^{a)}Electronic addresses: denbaars@engineering.ucsb.edu and volkan@stanfordalumni.org

in oxygen ambient to serve as both the transparent current spreading layer and the ohmic contact with the p-GaN layer. A mesa area of $350 \times 350 \mu\text{m}^2$ was defined using reactive ion etching (RIE) to expose the n-GaN layer. Finally, a Ti/Au bilayer with a thickness of 30 nm/150 nm was deposited as the metal contact pad to both the n-GaN and p-GaN layers.

The EL measurement was performed using a LED tester (Quatek M2442S-9 A). To exclude the thermal effect, a pulsed current source with a pulse duration of 5 ms at a repetition frequency of 20 Hz (duty-cycle 10%) was used. The micro-photoluminescence (μ -PL) measurements were performed at room temperature, and a He-Cd laser operating at 325 nm was used as the excitation source. The emission was collected by an objective lens (20 \times) and focused into an optical fiber and directed into a monochromator combined with a photomultiplier tube (Hamamatsu R928) for spectral recording. For the TRPL measurement, the excitation source was replaced by a pulsed Nd:YAG 4th harmonic (266 nm) laser with a pulse width of 1 ns at a repetition rate of 60 Hz. The detector output was recorded on a digital phosphor oscilloscope (Tektronix DPO 7254) and averaged over 500 periods to improve the signal-to-noise ratio. The electroabsorption spectra were recorded by employing a photocurrent setup consisting of a Xenon lamp, a monochromator, a chopper, a lock-in amplifier, a power meter, and a DC power supply.

The current-dependent emission peak wavelength and the full-width-at-half-maximum (FWHM) of both the polar and semipolar samples are presented in Fig. 1. As the current increases, the emission peak wavelength of the polar LED device is blue-shifted from 438.9 to 433.8 nm. This blue shift is attributed to the carrier-induced screening of the QCSE by the injected electrons and holes.^{9,10} For the semipolar LED sample, the emission peak wavelength exhibits a comparatively smaller blue shift, from 434.6 to 433.0 nm, with the increasing current from 5 to 50 mA. However, as the driving current goes beyond 50 mA, no further shift can be observed. Meanwhile, the semipolar LED sample presents a smaller broadening of FWHM compared to the polar LED sample with increasing current injection. Compared to the polar LED device, the semipolar LED device demonstrates a more stable EL emission. The different EL emission characteristics of the two samples are attributed to the different magnitudes of the

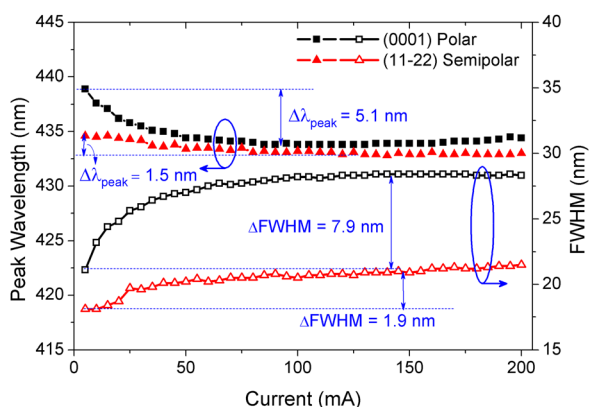


FIG. 1. Current dependence of electroluminescence emission peak wavelength and FWHM for the polar and semipolar GaN LED devices.

polarization induced internal electric field, which will be further confirmed in the following experiments.

The PL spectra of the polar and semipolar LED samples were captured with external voltage bias applied across the devices, as demonstrated in Figs. 2(a) and 2(b). For the PL spectra measured under the positive bias, the external voltage is kept well below the turn-on voltage to prevent the influence of the current injection. It is noted that the two samples display opposite shifting trends under the external bias. In Fig. 2(a), the PL spectra of the polar LED sample exhibit an obvious blue shift when negative biases from 0 to -2 V are applied across the device. When a positive voltage bias is applied, increasing from 0 to $+2$ V, the PL spectra is red-shifted correspondingly. In contrast, for the semipolar LED device, the PL spectra display a small red shift with the increasing negative external bias from 0 to -2 V, and a blue shift when the positive bias varies from 0 to $+2$ V as shown in Fig. 2(b). The opposite shifting trends reflect the opposite polarity of the internal electric fields in the two samples.

The TRPL spectra for both the polar and semipolar LED devices are shown in Figs. 3(a) and 3(b). The bias-dependent carrier lifetimes of both devices are extracted from the TRPL spectra and plotted in the insets. It is obvious that the polar LED device exhibits longer carrier lifetime than the semipolar LED device. In Fig. 3(a), when there is no bias applied across the device, the polar LED has a lifetime of 14.9 ns, about 2.7 times of that of the semipolar LED device, which is 5.5 ns. The polar LED device exhibits a prolonged decay process under positive external bias (0 to $+2$ V) and an accelerated decay when the bias is changed to negative voltages (0 to -15 V). The observed variation trend of the carrier lifetime is consistent with earlier studies reported.^{11,12}

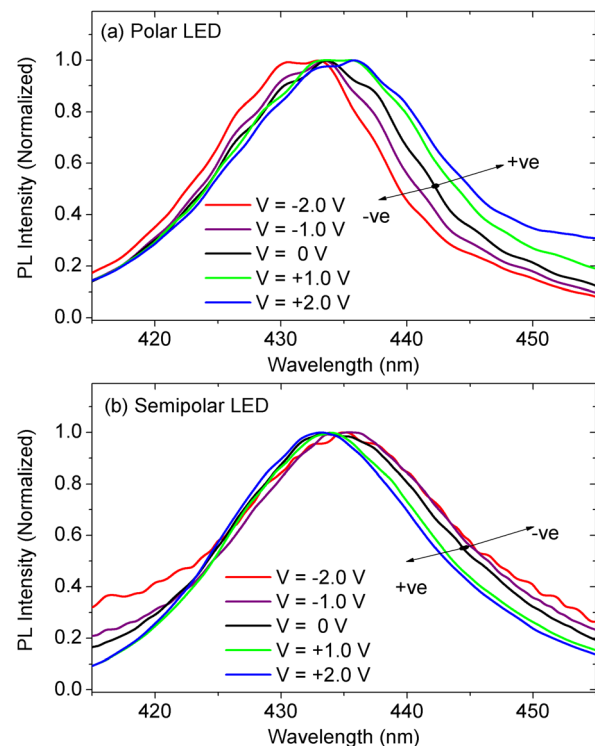


FIG. 2. Field-dependent photoluminescence spectra of (a) the polar LED device and (b) the semipolar LED device under the external bias from -2 to $+2$ V.

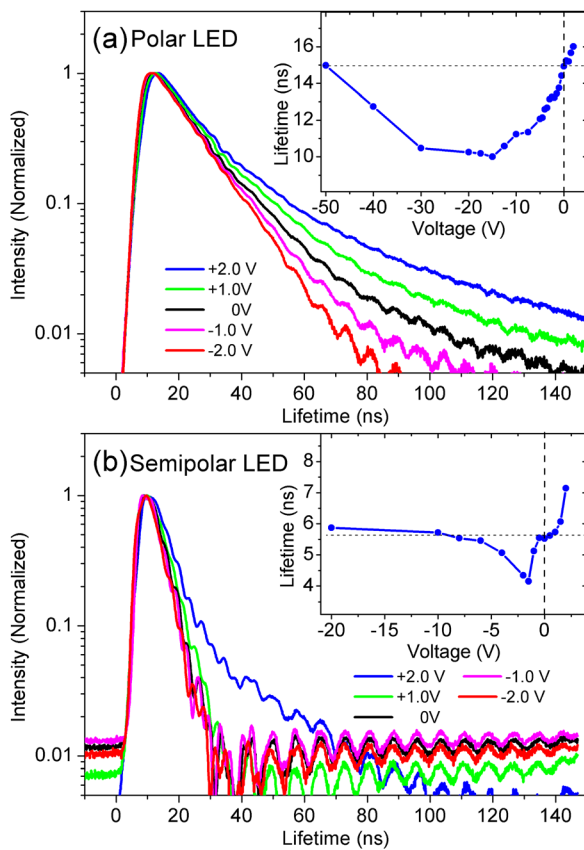


FIG. 3. TRPL spectra of (a) the polar LED device and (b) the semipolar LED device under external bias from -2 to $+2$ V. Inset shows the carrier lifetime (extracted using exponential fitting) for (a) the polar LED device under external bias from -50 to $+2$ V and (b) the semipolar LED device under external bias from -20 to $+2$ V.

The carrier lifetime reaches the minimum value of 10.0 ns under a negative bias of -15 V, indicating the fastest carrier decay process under this bias condition for the polar LED device. As the negative external bias is further increased, the decay is slowed down again, as reflected by the increased carrier lifetime. The TRPL spectra of the semipolar LED device exhibit a similar shifting trend under varying external bias conditions, as presented in Fig. 3(b). The shorter carrier lifetime at all bias voltage levels suggests higher recombination rates and, consequently, higher internal quantum efficiency. Besides, the semipolar LED device reaches the fastest decay time at a smaller negative bias voltage value of -1.5 V.

The electroabsorption spectra measured by the photocurrent for both the polar and semipolar LED devices are depicted in Figs. 4(a) and 4(b) with the photocurrent change relative to that under the zero-bias condition shown in the insets of the figures. For the polar LED device, due to the large polarization induced internal electric field, the efficiency of photon-generated carriers contributing to the photocurrent is very high, and the photocurrent can therefore reflect the absorption. The polar LED device presents a reduced absorption level at shorter wavelengths ($\lambda < 425$ nm) and slightly enhanced absorption in longer wavelength region ($\lambda > 425$ nm) when biased with positive voltages, as shown in Fig. 4(a). Under negative bias voltages of -1 and -2 V, the absorption coefficient is increased at short

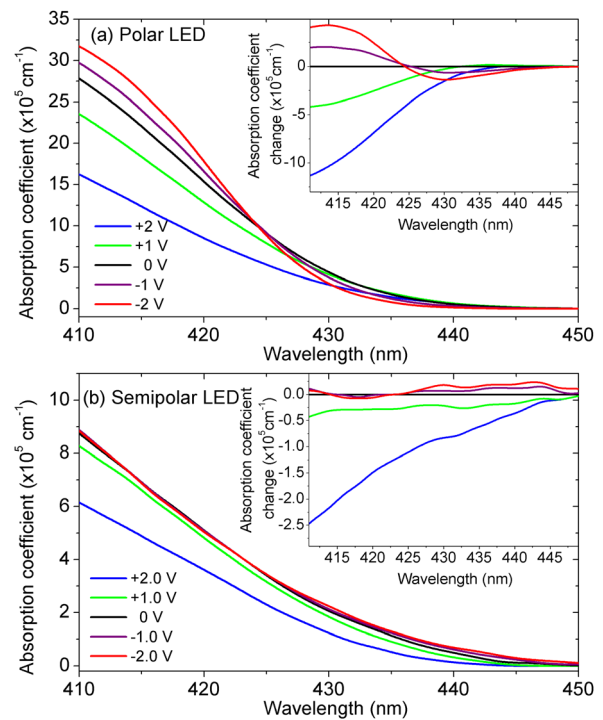


FIG. 4. Electroabsorption spectra of (a) the polar LED device and (b) the semipolar LED device under external voltage bias from -2.0 to $+2.0$ V. Inset: The absorption coefficient change compared to the zero bias condition.

wavelengths and is decreased at longer wavelengths. For the semipolar LED device under negative bias, due to the relatively large internal electric field, the photocurrent can be used to probe the absorption. It is found that the absorption at shorter wavelengths is decreased, while it is increased at longer wavelengths, just being opposite to the trend observed for the polar LED device. However, for the semipolar LED device under positive bias, the internal electric field is much smaller and the photo-generated electrons and holes have a larger chance to recombine before they are separated and transferred into the photocurrents. In this case, the photocurrent curve cannot accurately probe the absorption change for the semipolar LED device under the positive bias conditions.

The schematic energy band diagram in the InGaN/GaN QW is presented in Fig. 5 for both the polar and semipolar

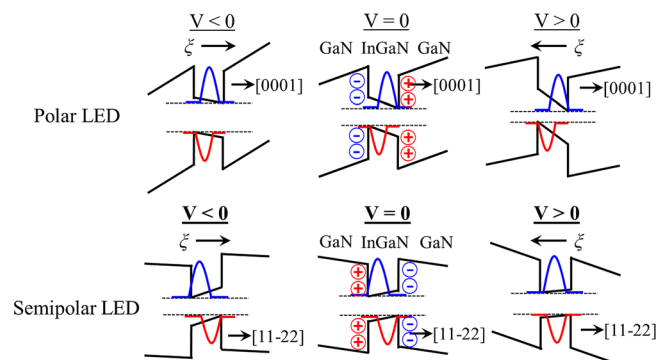


FIG. 5. Schematic energy band diagrams for polar and semipolar GaN LEDs with negative ($V < 0$), zero ($V = 0$), and positive ($V > 0$) external voltage bias.

LED devices. When there is no external bias applied to the device ($V = 0$ V), the QW of the polar LED device is subject to a polarization induced internal electric field, which is opposite to the direction of the [0001] growth orientation. Hence, the energy band within the QW is tilted by the internal electric field. Under positive voltage bias ($V > 0$), the external electric field is in the same direction with the internal electric field, leading to further tilting of the energy band of the QW and an enhanced QCSE. As a result, the effective band gap is reduced, as reflected in the red shift of the PL spectra in Fig. 2(a) and the reduced absorption at shorter wavelengths and the enhanced absorption at the longer wavelengths in Fig. 4(a). Meanwhile, the tilting of the energy band causes further separation of the electron and hole wave functions, resulting in a smaller likelihood for the electrons and holes to recombine. Therefore, the carrier lifetime becomes longer as compared to the zero bias condition as shown in Fig. 3(a). In contrast, when the polar LED is biased with negative voltages ($V < 0$), the external electric field is in the opposite direction with the internal electric field, making the energy band less tilted, and the QCSE is suppressed. Consequently, the effective energy band gap becomes wider, and the overlap between the electron and hole wave functions grows larger (improved likelihood for carrier recombination), as evidenced by the blue shift of the PL spectra in Fig. 2(a), the reduced carrier lifetime till -15 V in Fig. 3(a), and the absorption changes in Fig. 4(a). At a certain value of negative bias voltage, e.g., -15 V in this case, the external electric field is strong enough to fully offset the influence of the polarization field, leading to a flat energy band in the QW. Hence, the overlap between the carrier wave functions reaches the maximum, and the minimum carrier lifetime is obtained at this point. Consequently, the strength of the internal polarization electric field (ξ_{internal}) can be estimated at the flat band condition through

$$\xi_{\text{internal}} = \frac{V_{\text{bias}}}{d},$$

where V_{bias} is the voltage applied across the device, and d is the total thickness of the MQWs active layer region. In this case, ξ_{internal} is 2.0 MV/cm when d is taken as 75 nm. This value of the internal polarization electric field is consistent with the calculated theoretical values reported.¹³ This is therefore a convenient and simple experimental approach to indirectly measure the polarization induced internal electric field. As the negative bias is further increased, the energy band is tilted in the opposite direction, separating the electron and hole wave functions again. Correspondingly, the carrier lifetime is increased. As is known for the semipolar LED device, the [11 $\bar{2}$ 2] growth orientation is 58.4° away from the [0001] axis,^{14,15} the QW structure grown along this orientation experiences a weaker strain-induced polarization, and the polarization direction is opposite to the c -axis.¹⁶ Therefore, the energy band tilts less and along the opposite direction under the zero-bias condition, compared that of the polar LED device as shown in Fig. 5. With a positive bias voltage, the external electric field is in the opposite direction with the

internal field, making the energy band flatter. Hence, the effective band gap is increased, resulting in the blue shift of the PL emission. The negative bias condition provides an external electric field in the same direction with the internal field and causes the energy band to be further tilted. Therefore, the effective energy band gap becomes smaller, leading to a red shift of the PL emission. This agrees well with the shifting of the PL spectra observed in Fig. 2(b). Similar to the energy band analysis on the polar QW structure, the semipolar LED should display a shorter carrier lifetime under the positive bias, and a longer lifetime under reverse bias. However, the opposite trend has been observed here. This phenomenon is still not understood and under study at the moment. A trap-filling process could be a possible cause. Similar to the polar LED device, a flat band condition is also observed in the semipolar LED device but at a very small bias voltage of -1.5 V, which indicates a much smaller polarization induced internal electric field of 0.2 MV/cm.

In conclusion, this work studies the differences of carrier dynamics and emission kinetics within MQW LED structures grown on (11 $\bar{2}$ 2) semipolar plane and (0001) polar plane. Owing to the opposite polarity direction and the weaker polarization field, the LED structure grown on the (11 $\bar{2}$ 2) semipolar plane possesses a more stable electroluminescence performance and a faster lifetime decay. The investigation leads to a better understanding of the band structure and the recombination mechanisms of the multiple quantum wells structure and provides an insightful understanding for the LED based on non-polar and semipolar substrates.

This work was supported by the Singapore National Research Foundation under Grant No. NRF-CRP-6-2010-2 and NRF-RF-2009-09, and the Singapore Agency for Science, Technology and Research (A*STAR) SERC under Grant No. 112-120-2009.

- ¹Z. G. Ju, S. T. Tan, Z. H. Zhang, Y. Ji, Z. Kyaw, Y. Dikme, X. W. Sun, and H. V. Demir, *Appl. Phys. Lett.* **100**(12), 123503 (2012).
- ²Z.-H. Zhang, S. T. Tan, Z. Ju, W. Liu, Y. Ji, K. Zabu, D. Yilmaz, X. W. Sun, and H. V. Demir, *J. Disp. Technol.* **9**(4), 226 (2013).
- ³Y. Ji, Z.-H. Zhang, Z. Kyaw, S. T. Tan, Z. G. Ju, X. L. Zhang, W. Liu, X. W. Sun, and H. V. Demir, *Appl. Phys. Lett.* **103**(5), 053512 (2013).
- ⁴S. F. Chichibu, H. Yamaguchi, L. Zhao, M. Kubota, K. Okamoto, and H. Ohta, *Appl. Phys. Lett.* **92**(9), 091912 (2008).
- ⁵B. Liu, R. Zhang, Z. L. Xie, C. X. Liu, J. Y. Kong, J. Yao, Q. J. Liu, Z. Zhang, D. Y. Fu, X. Q. Xiu, H. Lu, P. Chen, P. Han, S. L. Gu, Y. Shi, Y. D. Zheng, J. Zhou, and S. M. Zhou, *Appl. Phys. Lett.* **91**(25), 253506 (2007).
- ⁶Y. Zhao, Q. Yan, C.-Y. Huang, S.-C. Huang, P. S. Hsu, S. Tanaka, C.-C. Pan, Y. Kawaguchi, K. Fujito, C. G. Van de Walle, J. S. Speck, S. P. DenBaars, S. Nakamura, and D. Feezell, *Appl. Phys. Lett.* **100**(20), 201108 (2012).
- ⁷H. Masui, S. Nakamura, S. P. DenBaars, and U. K. Mishra, *IEEE Trans. Electron Devices* **57**(1), 88 (2010).
- ⁸D. S. Kim, S. Lee, D. Y. Kim, S. K. Sharma, S.-M. Hwang, and Y. G. Seo, *Appl. Phys. Lett.* **103**(2), 021111 (2013).
- ⁹T. Takeuchi, C. Wetzel, S. Yamaguchi, H. Sakai, H. Amano, I. Akasaki, Y. Kaneko, S. Nakagawa, Y. Yamaoka, and N. Yamada, *Appl. Phys. Lett.* **73**(12), 1691 (1998).
- ¹⁰C.-F. Huang, C.-Y. Chen, C.-F. Lu, and C. C. Yang, *Appl. Phys. Lett.* **91**(5), 051121 (2007).
- ¹¹E. Sari, S. Nizamoglu, I.-H. Lee, J.-H. Baek, and H. V. Demir, *Appl. Phys. Lett.* **94**(21), 211107 (2009).

- ¹²Y. D. Jho, J. S. Yahng, E. Oh, and D. S. Kim, *Phys. Rev. B* **66**(3), 035334 (2002).
- ¹³O. Ambacher, J. Majewski, C. Miskys, A. Link, M. Hermann, M. Eickhoff, M. Stutzmann, F. Bernardini, V. Fiorentini, V. Tilak, B. Schaff, and L. F. Eastman, *J. Phys.: Condens. Matter* **14**(13), 3399 (2002).
- ¹⁴P. D. Mierry, N. Kriouche, M. Nemoz, S. Chenot, and G. Nataf, *Appl. Phys. Lett.* **96**(23), 231918 (2010).
- ¹⁵N. Okada, A. Kurisu, K. Murakami, and K. Tadatomo, *Appl. Phys. Express* **2**(9), 091001 (2009).
- ¹⁶A. E. Romanov, T. J. Baker, S. Nakamura, J. S. Speck, and E. J. U. Group, *J. Appl. Phys.* **100**(2), 023522 (2006).